

Mid-Infrared and X-ray luminosity correlations of X-ray point sources in NGC 1399

P. Shalima^{1*}, V. Jithesh², K. Jeena⁴, R. Misra¹, S. Ravindranath¹,
G. C. Dewangan¹, C. D. Ravikumar² and B. R. S. Babu³

¹ *Inter-University Centre for Astronomy and Astrophysics, Post Bag 4, Ganeshkhind, Pune-411007, India*

² *Department of Physics, University of Calicut, Malappuram-673635, India*

³ *Department of Physics, Sultan Qaboos University, Muscat, Oman*

⁴ *Department of Physics, Providence Womens' College, Malaparamba, Calicut-673009, India*

8 April 2019

ABSTRACT

It is known that the IR and X-ray luminosities of Active Galactic Nuclei (AGN) are correlated with $L_{IR} \sim L_X$. Moreover, the IR flux ratio between the 5.8 and 3.6 μm bands is a good distinguishing characteristic of AGN or AGN-like behaviour. On the other hand, Galactic X-ray binaries (GXB) are under-luminous in the IR with $L_{IR} \ll L_X$. Since Ultra-luminous X-ray sources in nearby galaxies may be an intermediate class between AGN and GXB, it is interesting to study if their IR properties indicate which kind of objects they resemble. We use Spitzer IRAC images to identify mid-IR counterparts of bright X-ray sources, detected by *Chandra* in the elliptical galaxy NGC 1399. We find that for sources with AGN-like IR flux ratios, the IR luminosity strongly correlates with that in X-rays, $L_{IR} \sim L_X$, while for the others, there is no correlation between the two. Some of the former objects may be background AGN. If they are not strongly contaminated by background AGN, this result extends the IR-X-ray luminosity correlation down to $L_X \sim 10^{39}$ ergs/s. We calculate their $g-z$ colours and find that the bright X-ray sources with IR counterparts are typically blue in optical color. This is in contrast to typical X-ray sources, without IR counterparts which have predominantly red optical counterparts. We highlight the need for IR or optical spectra of these sources to distinguish background AGN and unveil the effect of the X-ray emission on the different environments of these systems.

Key words: X-rays:binaries, infrared: general, ISM:dust, extinction

1 INTRODUCTION

Chandra and *XMM-Newton* have detected several off-nuclear X-ray point sources in nearby galaxies. Many of these sources are expected to be like typical X-ray binaries found in our Galaxy. However, unlike typical Galactic X-ray binaries (GXB), some of them have luminosities in excess of 10^{39} ergs s^{-1} and are called Ultra-Luminous X-ray sources (ULXs). As these ULXs have a luminosity higher than the Eddington limit for an accreting ten solar mass black hole, they may be harbouring black holes in the mass range of 100 - $10^5 M_\odot$ which are intermediate between the stellar mass black holes of Galactic X-ray binaries (GXB) and the super-massive black holes of Active Galactic Nuclei (AGN) (Colbert & Mushotzky 1999; Makishima et al. 2000). Spectral analysis of some ULXs seem to favour an IMBH interpretation, though not

conclusively (Miller et al. 2003; Miller, Fabian & Miller 2004; Devi et al. 2008). On the other hand, they could also be mildly beamed, super-Eddington accretion disks around stellar mass black holes as supported by recent spectral analysis (Shakura & Sunyaev 1973; King 2008; Kuncic et al. 2007; Feng & Soria 2011). Similar to GXB, some ULXs have exhibited spectral state transitions (Colbert & Mushotzky 1999; Kubota et al. 2001; Feng & Kaaret 2006) associated with changes in temporal behaviour (Dewangan et al. 2010). However, unlike GXB, the spectra of many ULXs exhibit a high energy cutoff at ~ 6 keV (Agrawal & Misra 2006; Dewangan, Titarchuk & Griffiths 2006; Stobbart, Roberts & Wilms 2006). Again, like GXB, a handful of ULXs exhibit quasi-periodic oscillations e.g., M 82 X-1 (Strohmayer & Mushotzky 2003), Holmberg IX X-1 (Dewangan, Griffiths & Rao 2006), NGC 5408 X-1 (Strohmayer et al. 2007), NGC 6946 X-1 (Rao, Feng & Kaaret 2010) and X42.3+59 (Feng, Rao & Kaaret 2010) at lower frequencies (~ 100

* E-mail: shalima.p@gmail.com (PS)

mHz), which indicates that they may indeed harbour IMBH. Thus, while the X-ray luminosity, spectral and temporal properties of a few ULXs suggest that they are intermediate objects between GXB and AGN, the definitive measurement of their black hole masses is yet to be made and hence their nature still remains largely mysterious. Moreover, since these X-ray sources are in general variable, some of the lower luminosity sources may be ULXs that have not been observed during their high flux period. It is important therefore, to study these sources at other wavelengths which may provide some distinguishing characteristics that can identify them to be more like AGN or GXB.

To understand the nature of the environment in which these X-ray sources are created, there have been extensive optical studies on the properties of the globular clusters that host an X-ray source (Kim et al. 2006, 2009). There have also been several studies and detections of optical counterparts of ULXs (e.g. Liu, Bregman & Seitzer 2004; Kuntz et al. 2005; Ramsey et al. 2006; Terashima, Inoue & Wilson 2006). While a few have been identified as O-type stars (Liu, Bregman & Seitzer 2002; Liu et al. 2007), the majority are star clusters (Goad et al. 2002; Ptak et al. 2006, e.g.). Unless its companion is a bright O-type star, an object similar to a GXB will be relatively faint in optical to be detected. For AGN including blazars, the ratio of the optical to X-ray flux can vary from 0.1-50 (Stocke et al. 1991). However, based on optical photometry alone (i.e. without detailed spectral information), it is difficult to discern and identify an AGN-like optically bright ULX, from a source in a globular cluster. Nevertheless, the absence of a bright optical counterpart for a ULX can be effectively used to impose a strong upper limit on the mass of the black hole, $M_{\text{BH}} < 1300M_{\odot}$ (Jithesh et al. 2011).

Another wavelength regime that could provide useful information regarding these sources is the infrared (IR). For GXB, the IR emission is correlated with the X-ray and is believed to originate from the companion star, the outer regions of the accretion disk and/or a jet (Russell et al. 2006). Harrison et al. (2011) have found periodic mid-IR emission in a LMXB GX17+2 which was consistent with synchrotron emission from the jet. For another LMXB GS 2023+338, Muno & Mauerhan (2006) found the mid-IR emission to be originating from dust in the accretion disc and follow the ν^{-2} law corresponding to the Rayleigh-Jeans tail of Black Body emission. However the IR luminosity is substantially weaker than the X-ray luminosity i.e. $L_{\text{IR}} \ll L_{\text{X}}$, and hence it is not detectable in extra-galactic sources.

The mid-IR (3-40 μm) emission in star-forming galaxies is also known to be correlated with X-ray emission but the mid-IR flux is 3-4 magnitudes higher than the X-ray and is dominated by PAH (Polycyclic Aromatic Hydrocarbon) emission (Symeonidis et al. 2011). This correlation exists even at small scales (Tyler et al. 2004) and is an indication of recent active star-formation (Kennicutt 1998).

A strong correlation between the X-ray and IR luminosities, $L_{\text{IR}} \sim L_{\text{x}}$ (e.g. Asmus et al. 2011; Krabbe, Böker & Maiolino 2001; Lutz et al. 2004) is also seen in AGN. Here the IR emission is due to reprocessing of the UV/X-ray emission from a dusty environment, except in jet-dominated blazars (Matsuta et al. 2012). The

difference in the ratio of the IR to X-ray luminosities of XRB and AGN, reflects a difference in the environment of these two types of sources, which may otherwise be black hole mass scaled versions of each other. AGN have red and featureless spectra in the mid IR (e.g. Houck et al. 2005; Hao et al. 2005; Weedman et al. 2005) and they have unique colours in this wavelength region which can be effectively used to identify them (Polletta et al. 2006; Lacy et al. 2004; Stern et al. 2005; Hatziminaoglou et al. 2005). For example, a positive flux ratio (in logarithmic units) between 5.8 and 3.6 μm bands implies that the IR emission is from an AGN (Lacy et al. 2004). The 5.8 μm channel contains the 6.2 μm PAH feature (Leger & Puget 1984; Allamandola, Tielens & Barker 1989) with only a 20% stellar contribution. On the other hand, the 3.6 μm channel consists mainly (> 90%) of stellar emission (Wang et al. 2004). Thus, such flux ratios may be taken as an indication of a dusty environment around a bright UV/X-ray source.

The IR emission of X-ray sources in nearby galaxies can provide valuable information regarding their environment. While some of them are expected to be similar to Galactic X-ray binaries where the IR is emitted from an outer disk or jet and having $L_{\text{IR}} \ll L_{\text{X}}$, there may be another type of sources where, like AGN, the IR may be due to reprocessed emission with $L_{\text{IR}} \sim L_{\text{x}}$. Moreover, since the IR-X-ray correlation in AGN, has been recently shown to extend to low luminosity AGN ($L_{\text{X}} \sim 10^{42}$ ergs/s), it is interesting to know whether there are sources at still lower X-ray luminosities ($L_{\text{X}} \sim 10^{37-40}$ ergs/s) for which the correlation holds.

Most of the IR studies of X-ray sources in nearby galaxies have been based on spectral studies. For 6 ULXs in NGC4485/4490, Vázquez et al. (2007) used Spitzer IRS spectra in order to derive IR spectral diagnostics that are characteristic of X-ray/UV heating of the surrounding gas and dust. They made use of the spectral resolution of the IRS instrument to estimate line ratios such as [NeIII]/[NeII] and [SIII]/[SiII] for the ULXs. These ratios, as suggested by Dale et al. (2006) are useful in separating accretion-powered from star-formation powered systems. Vázquez et al. (2007) found that 5 of the ULXs have these ratios similar to AGN while one of them may correspond to a star forming region. Vázquez et al. (2007) also modelled the continuum and derived dust temperatures for the sources, from which they suggested that for the two sources having hotter dust components, the [SiII] lines may be originating from the accreting source itself. Again, using the IRS instrument, Berghea et al. (2010a) detected [OIV] 25.89 μm emission from the ULX Holmberg II. Since this emission is associated with high excitation levels seen in AGN, it is an indication that the ULX is influencing its environment. By a detailed photo-ionization modelling of the IR lines, Berghea et al. (2010b) concluded that the luminosity and morphology of the [O IV] 25.89 μm emission line is consistent with photoionization by the soft X-ray and far ultraviolet (FUV) radiation from the accretion disk and inconsistent with narrow beaming. They also argued that in order to produce the observed [OIV] flux, the source should have a bolometric unabsorbed luminosity in excess of 10^{40} ergs s^{-1} .

While such detailed analysis can be undertaken if high resolution spectra are available, significant results can also be obtained by photometric measurements of IR counter-

parts of X-ray sources in nearby galaxies. Since the IR photometric data can be obtained for a larger number of X-ray sources in a galaxy, one can study statistical properties such as whether the X-ray luminosity correlates with the IR or not. To identify IR counterparts of X-ray sources unambiguously, the host galaxy should have a smooth continuum IR profile which can be modelled and subtracted out, to reveal the true point-like IR sources. Thus, a nearby elliptical galaxy which hosts a large number of X-ray sources would be ideal for such a study. NGC1399 is a bright elliptical galaxy in the centre of the Fornax cluster. It is unique in having a large number of X-ray sources with a significant fraction of them being ULXs (Swartz et al. 2004). Angelini, Loewenstein & Mushotzky (2001) have studied the X-ray sources in this galaxy and found that about 70% of them are associated with globular clusters, which implies that the X-ray sources are formed preferentially in globular clusters.

In this paper, we have analysed archival data of NGC1399 from Spitzer IRAC and *Chandra*, in order to study the IR counterparts of the X-ray sources in the galaxy. We have used the IR photometric flux ratios to identify AGN-like sources and to see if the IR flux is correlated with that of the X-rays as seen in AGN.

2 X-RAY AND INFRARED DATA ANALYSIS

2.1 Chandra data

We have analysed a 56 ksec *Chandra* observation (ID : 319) of NGC 1399. The data reduction and analysis were done using CIAO 4.2, and HEASOFT 6.9.0. Using the CIAO source detection tool *celldetect*, a total of 120 X-ray point sources were extracted from the level 2 event list with *signal-to-noise* ratio of 3. Of these 120 sources, 118 were within the field of view of the Spitzer IRAC observation and hence these sources were considered as the sample.

For some of the 118 point sources, the net X-ray count is too small ($N_C < 50$) for spectral analysis. Moreover, some sources, typically near the galaxy centre, are in regions of excessive diffuse emission. Taking these aspects into consideration, we were able to extract reliable spectra for 35 sources (Tables 1,2,and 3) out of a total of 118 which were in the FOV. The spectral analysis was done using XSPEC version 12.6.0, and the data were fitted in the energy range of 0.3 – 8.0 keV. The inferred luminosity of a source depends on the spectral model used and hence following Devi et al. (2008), we fitted each source independently with an absorbed powerlaw and an absorbed disk blackbody spectral model. The model which provided a lower χ^2 was considered as a better representative and the corresponding X-ray luminosity was ascribed to that source. Two of these sources required an additional diffuse thermal component which was modelled using the XSPEC model, mekal. For the rest of the sources, the X-ray counts are taken to be a proxy for the luminosity of the source. For example, Angelini, Loewenstein & Mushotzky (2001) considered the X-ray sources of this galaxy and estimated a conversion factor between the count rate and luminosity. This assumes that the faint sources have roughly the same spectra and can be represented by a power-law absorbed by Galactic absorption.

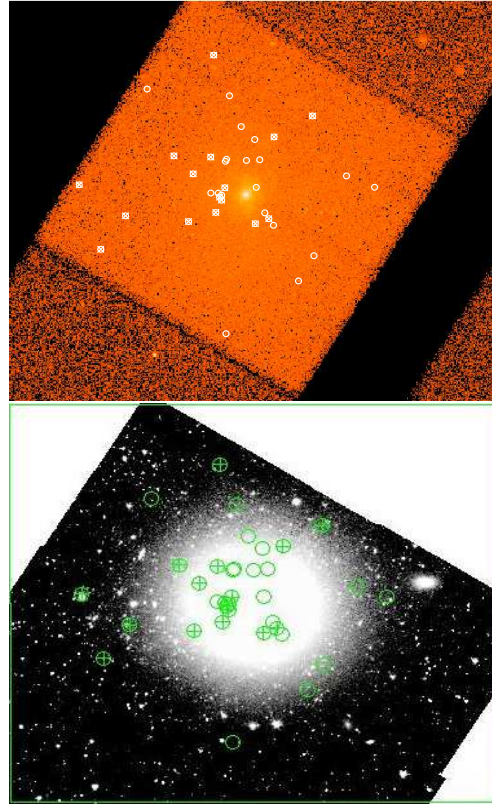


Figure 1. *Chandra* (above) and *Spitzer* (below) image of NGC1399 with the X-ray sources with spectra (circles) and their IR counterparts (crosses) marked. The size of the images are 12 by 10 arcminutes

2.2 Spitzer IRAC

The IRAC instrument on board Spitzer provides mid-IR images at four wavelengths i.e. 3.6, 4.5, 5.8 and $8\mu\text{m}$. The IRAC Post Basic Calibrated Data (PBCD) mosaic files of NGC1399 were obtained from the Spitzer Heritage Archive. We have used the data corresponding to AOR 5529856 which was part of the Spitzer Infrared Nearby Galaxies Survey (Kennicutt et al. 2003). The exposure time was 840 seconds.

We used the X-ray positions of 118 X-ray sources near NGC1399 in order to look for IR counterparts. Out of the four wavelengths, 3.6 and $5.8\mu\text{m}$ were used in this analysis as only they had good coverage of locations of X-ray point sources.

We used the $3.6\mu\text{m}$ image which has the highest spatial resolution and extracted sources at the 3-sigma level using the Source Extractor package of Bertin & Arnouts (1996). For sources which would otherwise be undetectable against the bright image of the galaxy, an isophotal model of the elliptical galaxy was subtracted from the original image using the IRAF package before extracting point sources.

At the 3-sigma level, the source extractor detected 827 IR sources in the $3.6\mu\text{m}$ image of NGC 1399 over an area covering 12 by 10, which covers the coordinates of 118 X-ray point sources (Figure 1). Thus the average number density of sources in the field is $\sim 1.9 \times 10^{-3}$ sources/arcsec². The relative astrometry between *Chandra* and HST is around 1.5 arcsecs and the size of the

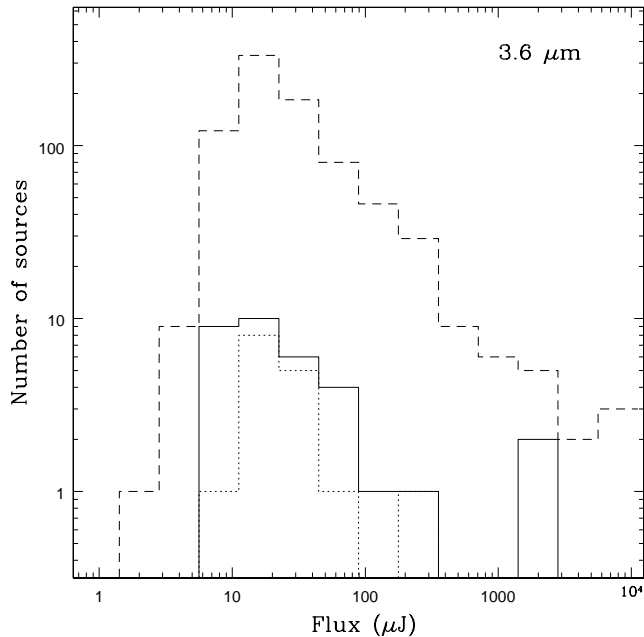


Figure 2. Histogram of the IR luminosities of all sources detected in the IRAC image (dashed line) and the counterparts of X-ray point sources (solid line). The K-S test statistic is $d=0.15$ with a probability of 0.43. Sources with X-ray spectra are indicated by the dotted line. The K-S test statistic for these sources is $d=0.13$ (prob = 0.92).

Chandra point spread function is around 0.5 arcsecs (e.g. Angelini, Loewenstein & Mushotzky 2001). Here, we assume that the relative astrometry between *Chandra* and *Spitzer* is around 2 arcsecs and look for the IR counterparts of the X-ray sources. The probability that an IR source will fall within 2 arcsecs of an X-ray coordinate by chance is roughly the IR source density times the area of a circle of 2 arcsec i.e. $\sim 2.4\%$. Of the 118 X-ray sources considered we may expect around 3 of them to have an IR source within 2 arcsecs just by chance. Instead, we find that 33 of them have an IR counterpart. This implies that most of the IR counterparts are real and not chance coincidences. Figure 1 show the *Chandra* and *Spitzer* images of the region with the X-ray sources and their IR counterparts marked.

For all IR sources we used the APEX software available at the *Spitzer* website in order to derive the aperture fluxes as well as the uncertainties inside the extraction aperture. The flux uncertainties were obtained from error maps that were downloaded from the *Spitzer* website.

For the aperture photometry, we used an aperture of radius 1.44'' and 1.49'', twice the FWHM of the 3.6 and 5.8 μ m channels respectively. For the X-ray sources that are not detected at 3.6 μ m, we quote the 3-sigma upper limits at the locations. Luminosities ($\nu F_\nu \times 4\pi D^2$) were then calculated using the distance to NGC 1399 to be $D = 19$ Mpc. The NASA/IPAC Extragalactic Database (NED) shows that there are a large number of distance estimate for NGC 1399 ranging from 13.8 to 24.9 Mpc, and hence we have taken the average value of 19 Mpc.

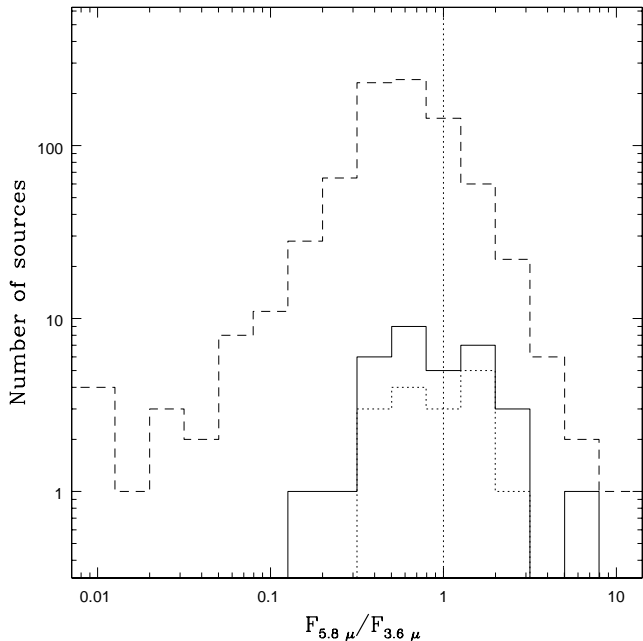


Figure 3. Histogram of the IRAC colours of all sources detected in the IRAC image (dashed line) and the counterparts of X-ray point sources (solid line). Also plotted is the histogram for the 16 sources with X-ray spectra ($N_C > 50$), which have detected mid-IR counterparts (dotted line). The vertical line demarcates the AGN-like from the non AGN-like sources.

3 SOURCE DISTRIBUTIONS

In this section, we compare the distributions of all the IR and X-ray point sources in the sample and compare them with those that have an IR/X-ray counterpart. This is useful to see if the sources which are bright in both IR and X-rays are different from the parent distribution. However, we note that neither the IR nor the X-ray source sample used is complete. There are IR sources considered which are not in the *Chandra* field of view. More importantly, detection of IR and X-ray point sources depends on the level of the background diffuse emission at that location and for *Chandra* the off axis efficiency of point source detection is different than the on-axis one. Our interest here is to check whether on an average the properties of sources that are IR counterparts of X-ray sources, differ from the remaining sources identified in the IR images.

Figure 2 shows the histogram of the IR 3.6 μ m flux for all 827 sources in the field (dashed line) and that of the 33 IR sources detected in X-rays (solid line). A Kolmogorov-Smirnov (K-S) test, reveals that there is no significant difference between the two distributions with K-S statistic $d = 0.15$ corresponding to a probability of 0.43. Throughout this work we consider a probability of 0.05 or less to be significant. The dotted line in the figure shows the distribution of the 16 IR sources with X-ray counts $N_C > 50$, and that distribution is also not different from the parent one with $d = 0.13$ corresponding to a probability of 0.92. Thus in terms of IR flux, there is nothing special about the IR sources having bright X-ray emission.

AGN have unique colours in the mid-IR range and in

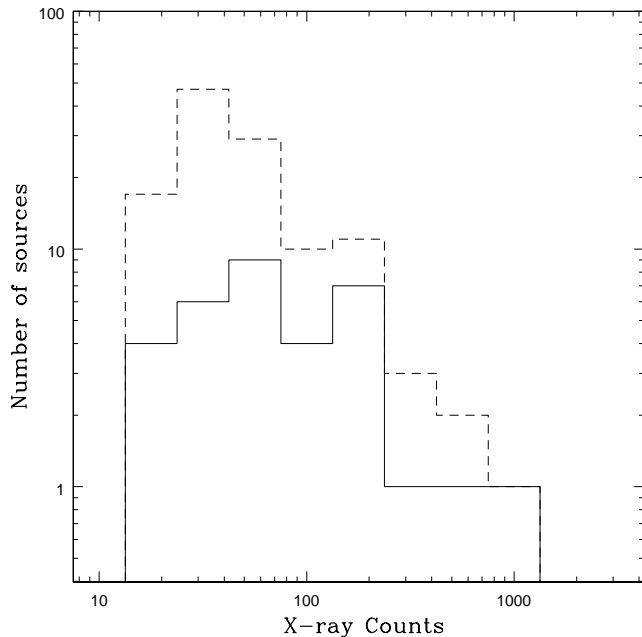


Figure 4. Histogram of X-ray counts for the X-ray point sources (dashed Line) and their IR counterparts.

particular the IRAC flux ratio between the 5.8 and $3.6\mu\text{m}$ bands, $F_{5.8}/F_{3.6} > 1$ is a good identifier (Lacy et al. 2004). Figure 3 shows the histogram of this ratio for the field 827 IR sources (dashed line) and for the 33 sources with X-ray emission (solid line). The two distributions are significantly different with a K-S statistic $d = 0.29$ corresponding to a probability of 0.006 (assuming a level of significance of 0.05). This difference is primarily because the fraction of IR sources that are X-ray bright with $F_{5.8}/F_{3.6} > 1$ is $\sim 10\%$ as compared to $\sim 5\%$ for those that have $F_{5.8}/F_{3.6} < 1$. The dotted line represents the 16 sources with X-ray counts, $N_C > 50$ which indicates that they have similar IR flux ratio as sources with $N_C < 50$.

Next, we checked the X-ray intensity (or counts) of the X-ray sources that have IR emission. Figure 4 shows the distribution of the 118 X-ray point sources (dashed line) compared with the 33 sources with IR emission. The K-S statistic is $d = 0.24$ with a probability of 0.089.

Thus, although the probability of an IR point source to be X-ray bright does not seem to depend on the IR flux, it increases with the IR flux ratio $F_{5.8}/F_{3.6}$. Moreover a brighter X-ray point source is slightly more likely to have an IR counterpart than a fainter one.

4 X-RAY IR CORRELATIONS

Figure 5 shows the IR $3.6\mu\text{m}$ luminosity, $L_{IR(3.6)}$ ($\equiv \nu F_{\nu} 4\pi D^2$) v/s X-ray counts for the 33 X-ray point sources with IR point source counterparts. Overall there does not seem to be any correlation. However, for sources with AGN-like IR color i.e. $F_{5.8}/F_{3.6} > 1$ (circles) the Spearman rank correlation (significance level = 0.05) co-efficient is 0.49 which corresponds to a probability of 0.06. When we consider only brighter sources with X-ray counts > 50 , the rank

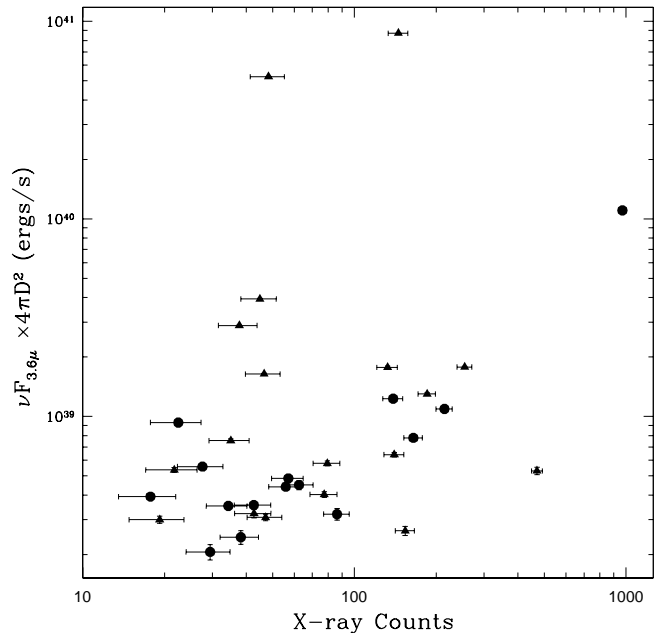


Figure 5. IR($3.6\mu\text{m}$) Luminosities v/s X-ray counts for the IR counterparts. The points with positive ($\log(F_{5.8}/F_{3.6})$) and negative ratios are shown as circles and triangles respectively. The Spearman Rank correlation co-efficients are 0.49 (prob=0.06) and 0.12 (prob=0.65) respectively. For sources with X-ray counts greater than 50, the co-efficients become 0.76 (prob=0.03) and 0.17 (prob=0.67).

probability decreases to 0.03. Sources that do not have AGN-like colours i.e. $F_{5.8}/F_{3.6} < 1$ (triangles) do not show any significant IR-X-ray correlation with a Spearman Rank correlation co-efficient of 0.12 and probability of 0.65.

Out of the 35 X-ray bright sources with spectra, 16 of them have mid-IR counterparts (see Figure 1). We compared the IR $3.6\mu\text{m}$ with the unabsorbed X-ray luminosities for eight of the sources that have AGN-like colours in Figure 6. The Spearman rank correlation is significantly better (assuming a significance level of 0.05) with a probability of 0.002 in contrast to 0.007 when X-ray counts are considered instead of the luminosity. Moreover, the correlation is given by

$$\frac{L_X}{10^{39}\text{ergs/s}} = (0.72 \pm 0.06) \left(\frac{L_{IR(3.6)}}{10^{39}\text{ergs/s}} \right)^{0.90 \pm 0.04} \quad (1)$$

with a reduced $\chi^2 = 0.86$. In contrast, fitting $L_{IR(3.6)}$ with X-ray counts, using the same parametric function gives a reduced $\chi^2 = 10.74$.

For eight sources which do not have AGN-like IR colours, the X-ray and the $3.6\mu\text{m}$ IR luminosities do not correlate with each other as shown in the top panel of Figure 7.

Also for the AGN-like sources, the $5.8\mu\text{m}$ luminosity is correlated with the X-ray luminosity (circles in Figure 8) and is given by

$$\frac{L_X}{10^{39}\text{ergs/s}} = (0.76 \pm 0.1) \left(\frac{L_{IR(5.8)}}{10^{39}\text{ergs/s}} \right)^{0.89 \pm 0.06} \quad (2)$$

which is consistent with the best fit parameters for $3.6\mu\text{m}$.

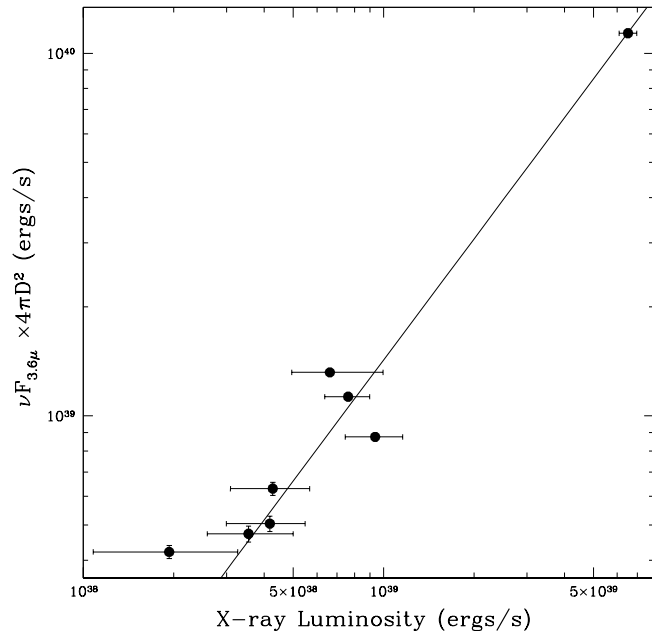


Figure 6. IR(3.6μ) ν/s unabsorbed X-ray luminosities for sources with positive ($\log(F_{5.8}/F_{3.6})$) ratios. The correlation coefficient is 0.91 (prob=0.002). Excluding the most luminous object at 3.6μ , the correlation co-efficient becomes 0.86 (prob=0.01).

However, the fit is not as good here with a reduced $\chi^2 = 2.16$. There is no such correlation seen between the the 5.8μ and the X-ray luminosity for the eight sources without AGN-like colours (triangles in Figure 8).

For the remaining 19 bright X-ray sources there is no IR counterpart detected at the 3-sigma level. Figure 7, shows the distribution of upper limits on the IR luminosities of these sources versus the X-ray luminosity.

We have also looked for correlations of the IR flux with X-ray hardness ratios for the 16 detected IR sources. Figure 9 shows the plot of the hardness ratio against the 3.6μ fluxes. The Rank correlation co-efficient is -0.42 with a probability of 0.1 indicating a lack of correlation between the two.

5 OPTICAL COUNTERPARTS IDENTIFIED FROM HST DATA

The Optical analysis of NGC 1399 was carried out using the archival images of HST with Advanced Camera for Survey (ACS). Among the archival data sets, the observations with longer exposure time and multiple filters, especially the wide band filters (F814W, F475W, F850LP and F606W) were considered for the analysis. Images in different pointings were also taken to have the maximum number of X-ray sources in the field of view. To overcome the effect of the varying host galaxy background intensity on the detection and photometry of the point sources, a smooth model of the galaxy was subtracted from the observed image. The smooth model was generated by fitting elliptical isophotes to the brightness distribution of the galaxy using the ELLIPSE task in IRAF/STSDAS. The other brighter objects near the

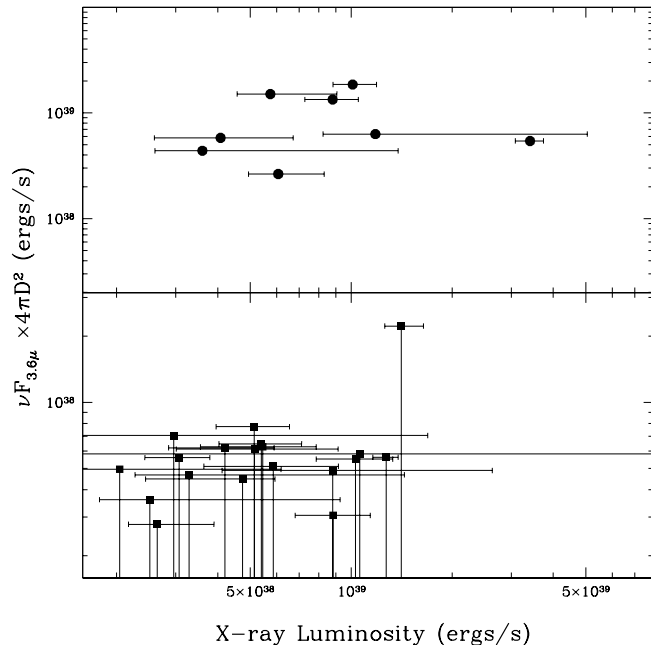


Figure 7. IR(3.6μ) ν/s unabsorbed X-ray luminosities for sources with positive ($\log(F_{5.8}/F_{3.6})$) ratios (above) and the 3-sigma upper limits for the 19 locations without IR counterparts (below). The correlation co-efficient is 0.29 (prob = 0.49).

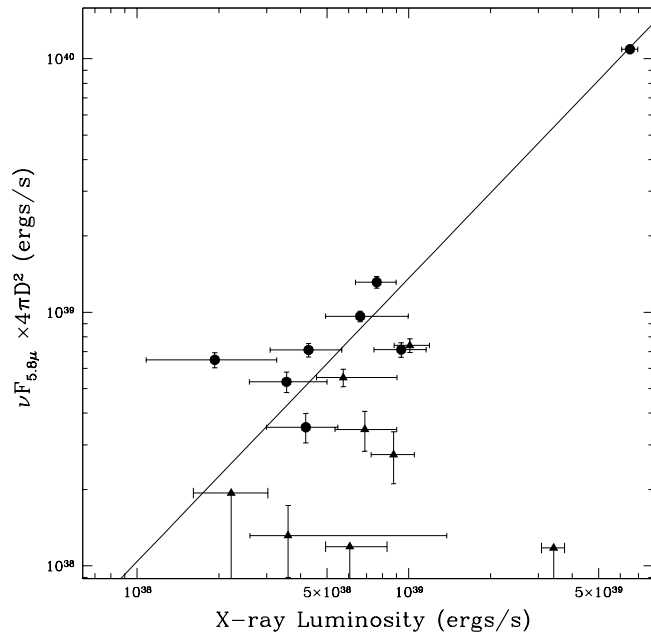


Figure 8. IR(5.8μ) ν/s unabsorbed X-ray luminosities. The points with positive ($\log(F_{5.8}/F_{3.6})$) and negative ratios are shown as circles and triangles respectively. The Rank correlation co-efficient for all the sources is 0.29 (prob=0.27). For the sources with positive and negative flux ratios, the co-efficients are 0.83 (prob=0.01) and 0.02 (prob=0.96) respectively. 3-sigma upper limits are plotted for the sources with fluxes less than this value .

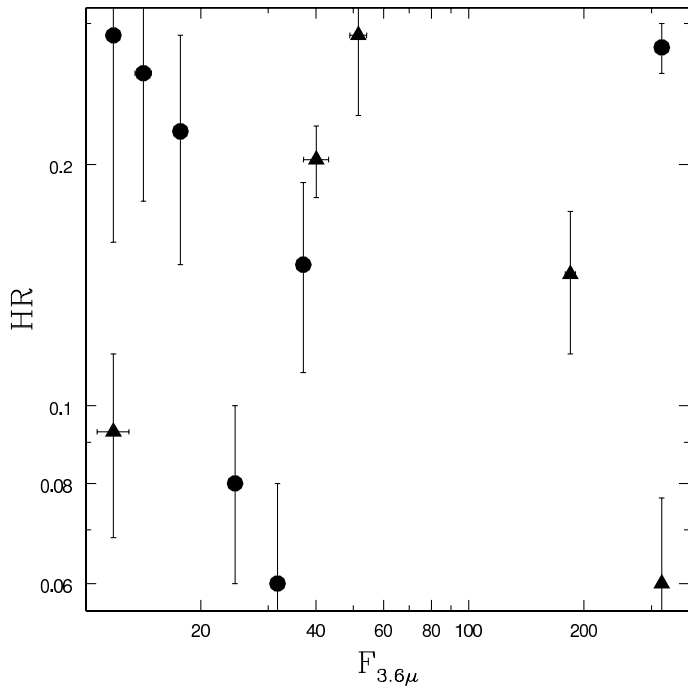


Figure 9. IR(3.6μ) fluxes v/s X-ray hardness ratios. The points with positive ($\log(F_{5.8}/F_{3.6})$) and negative ratios are shown as circles and triangles respectively. The Rank correlation co-efficient for all the sources is -0.42 (prob= 0.10) .

galaxy were masked during the fitting. The model image was subtracted from the observed image (F814W) to get the residual image. The object extraction was carried out on the residual image using SExtractor, to detect and extract the sources for the 3-sigma detection threshold. When images are available in multiple filters and different pointings, one of the optical image is taken as the reference image (Obs ID : J9P305010) and the other images are aligned to the reference one using GEOMAP and GEOTRAN tasks in IRAF. We find that 26 of the *Chandra* X-ray sources are within the field of view of available HST data sets and 21 sources have an optical counterpart at least in one filter, within a positional offset of less than one arc-second. This constant offset was applied to the *Chandra* source positions, thereby matching these shifted sources with the optical sources in the SExtractor catalogue. There are five X-ray sources which do not have optical counterparts (at the 3-sigma level) within one arc second of their shifted positions and are *optically-dark* X-ray bright sources (Jithesh et al. 2011).

6 OPTICAL PHOTOMETRY

Photometry of the identified optical counterparts of X-ray point sources were performed on the drizzled image using the apphot package in IRAF. The drizzled images, which are in units of $e^-/s/pixel$, are converted to e^- per pixel by multiplying by the total exposure times. An aperture of radius 10 pixels was used to extract the flux in the task APPHOT and the Vega magnitude was computed with zero points taken from *HST ACS* data handbook. For the optically dark sources, we estimated the upper limit on their

optical flux based on the 3-sigma detection threshold at that position.

7 OPTICAL COLOURS

We have calculated the $g-z$ optical colours for 17 of the 35 X-ray bright sources. Paolillo et al. (2011) define the range ($1.3 < g-z < 2.5$) for which they consider an optical source to be a globular cluster. In our sample, 16 of the 17 sources with color information may be globular clusters according to this criterion. Moreover, 7 of these 16 sources are blue ($1.3 < g-z < 1.9$) while the rest 9 are red ($1.9 < g-z < 2.5$). Paolillo et al. (2011) reported that the majority of the X-ray sources reside in red globular clusters. However, it seems that for the bright X-ray sources considered here, a significant fraction of them are located in the blue clusters. Of the 8 X-ray sources with AGN-like IR colours (Table 1), 4 of them have $g-z$ values, and 3 of them are optically blue and one is red. Of the 8 sources which have non-AGN-like IR colours (Table 2), 5 of them have $g-z$ values. Here one is extremely blue ($g-z \sim 1$), two are blue ($g-z \sim 1.8$) and the other two are red ($g-z > 2$). Thus, these results indicate that although in general X-ray sources primarily reside in red globular clusters (Paolillo et al. 2011), the optical colours of sources with IR counterparts are primarily blue. This is particularly true for those sources which have AGN-like IR colours.

We have also compared the positions of the sources with the known Ultra Compact Dwarf Galaxies near NGC 1399, and found that none of these X-ray sources can be identified with them.

8 CONTAMINATION BY BACKGROUND AGN

It is possible that some of the X-ray sources considered in this work are distant background AGN since 40% of the X-ray sources in elliptical galaxies are found to be background objects (Swartz et al. 2004; Paolillo et al. 2011). This is particularly true for the 8 bright X-ray sources which have IR counterparts with AGN-like colours. If we assume a contamination of 40% we find that 7 of the 16 sources could be background AGN and then the X-ray/IR correlation is just a manifestation of the known correlation for AGN (Asmus et al. 2011). Indeed, the fact that three of the four sources which have measured optical colours are blue, further indicates that they may be background AGN. If that is so, the IR flux ratio of the infra-red counterparts can be used as a good discriminator to distinguish background AGN from the X-ray sources within the galaxy. Following this argument, the X-ray bright sources that belong to the host galaxy would have non-AGN IR colours. For example, one of the ULX (Source no. 9, see Table 2) with an X-ray luminosity of $\sim 3.4 \times 10^{39}$ ergs/s has non-AGN like IR color, and its optical counterpart is consistent with being a red globular cluster. However, there are some indications that several of the sources showing AGN-like colours may not be background AGN. For example, the source no. 6 (Table 1) has IR flux ratio expected for AGN, but has red optical colours. We

analysed the Spitzer IRAC image of NGC 4485/4490 and detected two of the sources studied by Vázquez et al. (2007) in both the IRAC wavelength channels ($3.6\mu\text{m}$ and $5.8\mu\text{m}$). For both these sources $F_{5.8}/F_{3.6} > 1$ indicating that they have AGN-like colours. Using emission line ratios, Vázquez et al. (2007) classified one of these sources as AGN-like and the other as a supernova remnant. The only decisive way to determine whether these objects are in the galaxy or background AGN is to obtain high quality spectra in IR/optical.

9 DISCUSSION

We have analysed the Spitzer/IRAC images at $3.6\mu\text{m}$ and $5.8\mu\text{m}$ to identify mid-IR counterparts of the X-ray sources in NGC 1399. We considered the 35 bright X-ray sources for which the X-ray counts are high enough to perform reliable spectral modelling and estimate the X-ray luminosities. We find that 16 of them are detected in the IR (see Figure 1). We have used the mid-IR colours of these IR sources to classify them into AGN-like and non-AGN-like sources. We find that for 8 sources that have AGN-like ($F_{5.8}/F_{3.6} > 1$) colours, the X-ray luminosities correlate well with the mid-IR luminosities as is the case for AGN. On the other hand the X-ray and mid-IR luminosities of the remaining sources do not show any correlation.

Using the optical colours, we find that the AGN-like counterparts are mostly blue in contrast to the general X-ray sources that have preferentially red optical colours. While it appears that AGN-like IR flux ratios and blue optical colours can potentially be used to identify the background AGN, we cite the case of X-ray sources in NGC 4485/4490 where there are off-nuclear X-ray sources belonging to the host galaxy which exhibit AGN-like IR colours. The background AGN can only be reliably identified by spectral analysis.

In case a majority of the sources are AGN we re-affirm that mid-IR colours can be used as a good technique to differentiate AGN from other X-ray sources. However it is possible that the majority of them are sources in the galaxy itself. If this is the case, we extend the $L_{\text{IR}}-L_{\text{X}}$ correlation of Asmus et al. (2011) down to X-ray luminosities of 10^{39} ergs s^{-1} .

Another possibility is the contamination from nearby star-forming regions which could also show a correlation between IR and X-ray luminosities. However, this is highly unlikely in this case since there is no evidence for star-formation in NGC1399. Also for star-forming galaxies the IR fluxes are found to be much higher than their X-ray fluxes, while they are of the same order here.

In summary, our study of the mid-IR counterparts of X-ray sources shows that there are two categories of bright X-ray sources, one where the mid-IR luminosity correlates with the X-ray like AGN and the other where the IR and X-ray luminosities are uncorrelated. This indicates a possible difference in the environment of these two sources, i.e. one which has a dusty environment, other being dust deficient. The difference in the two classes of X-ray sources is further highlighted by optical photometry which suggests that bright X-ray sources that are AGN-like are bluer than typical X-ray sources which are red. This again perhaps indicates either a difference in environment or in the nature of the globular cluster that hosts the two classes.

However, as mentioned earlier these results need further investigations through IR spectroscopy to confirm what fraction of sources are background AGN or belong to the galaxy. The sources identified in this work are potential candidates for further spectroscopic follow-up studies. Moreover there is a need for a comparative study with other elliptical galaxies which will help us understand whether they host two classes of X-ray sources as seen in the case of NGC 1399. Also, a larger sample in different galaxies could give a better understanding on the nature of the two classes of X-ray sources.

ACKNOWLEDGEMENTS

We thank the referee for useful suggestions and comments which helped us to greatly improve the manuscript. V.J., K.J., C.D.R., and B.R.S.B. thank the IUCAA visitors program and UGC Special assistance program. This work has been partially funded from the ISRO-RESPOND program. The authors thank Phil Charles for useful discussions. V.J. acknowledges financial support from the Council of Scientific and Industrial Research (CSIR) through SRF scheme. P.S. would like to thank Calicut University for their support and hospitality. This work is based [in part] on observations made with the Spitzer Space Telescope, which is operated by the Jet Propulsion Laboratory, California Institute of Technology under a contract with NASA.

Table 1. Properties of mid-IR counterparts with positive $\log(F_{5.8}/F_{3.6})$ ratios.

No (1)	R.A. (2)	Dec. (3)	m_{814W} (4)	m_{475W} (5)	m_{850LP} (6)	m_{606W} (7)	L_X (8)	χ^2/dof (9)	$3.6\mu\text{m}$ (10)	$5.8\mu\text{m}$ (11)	$F_{5.8}/F_{3.6}$ (12)	$g-z$ (13)
1	3 38 51.61	-35 26 43.59	-	-	-	19.89±0.001	39.81 ^{+0.03} _{-0.02}	55.78/58	319.11 ± 1.70	492.78 ± 4.78	0.18	-
2	3 38 25.29	-35 25 21.92	-	-	-	20.11±0.001	38.88 ^{+0.07} _{-0.08}	14.24/13	31.73 ± 0.71	59.42 ± 3.10	0.27	-
3	3 38 33.12	-35 27 31.29	20.698±0.005	21.806±0.007	20.499±0.008	21.418±0.004	38.97 ^{+0.09} _{-0.10}	20.47/11	24.58 ± 0.59	32.19 ± 2.10	0.12	1.307
4	3 38 45.35	-35 27 37.07	-	-	-	24.575±0.031	38.82 ^{+0.18} _{-0.13}	6.69/6	37.03 ± 0.46	43.62 ± 2.09	0.07	-
5	3 38 25.94	-35 27 41.77	25.729±0.00	26.773±0.00	25.437±0.00	27.383±0.00	38.55 ^{+0.13} _{-0.14}	2.37/3	13.28 ± 0.67	25.04 ± 2.21	0.28	-
6	3 38 32.34	-35 27 10.34	21.335±0.013	23.160±0.022	20.973±0.014	22.342±0.011	38.63 ^{+0.12} _{-0.14}	0.26/6	17.70 ± 0.73	32.11 ± 1.95	0.26	2.187
7	3 38 27.76	-35 27 50.2	22.983±0.045	24.194±0.049	22.818±0.055	23.926±0.033	38.62 ^{+0.12} _{-0.15}	13.06/9	14.17 ± 0.70	15.92 ± 2.12	0.05	1.376
8	3 38 36.17	-35 26 25.11	21.429±0.008	22.528±0.010	20.872±0.009	21.760±0.004	38.29 ^{+0.23} _{-0.25}	4.40/4	11.84 ± 0.50	29.34 ± 2.00	0.39	1.656

Note. — (1) Source Number; (2) Right Ascension (J2000); (3) Declination (J2000); (4)-(7) Vega magnitudes in the HST F814W, F475W, F850LP and F606W filters; (8) unabsorbed X-ray luminosity (ergs/s); (9) χ^2 value for X-ray model used to estimate the luminosity; (10), (11) IR flux in MJy for the $3.6\mu\text{m}$ and $5.8\mu\text{m}$ bands; (12) mid-IR flux ratio; (13) optical ($g-z$) color. The ‘-’ sign denotes the cases where sources are not in the FOV of the HST image.

Table 2. Properties of mid-IR counterparts with negative $\log(F_{5.8}/F_{3.6})$ ratios.

No (1)	R.A. (2)	Dec. (3)	m_{814W} (4)	m_{475W} (5)	m_{850LP} (6)	m_{606W} (7)	L_X (8)	χ^2/dof (9)	$3.6\mu\text{m}$ (10)	$5.8\mu\text{m}$ (11)	$F_{5.8}/F_{3.6}$ (12)	$g-z$ (13)
9	3 38 32.60	-35 27 5.12	20.373±0.005	22.271±0.010	20.059±0.007	21.377±0.004	39.53 ^{+0.04} _{-0.04}	47.68/39	15.25 ± 0.68	< 5.31	< -0.45	2.21
10	3 38 48.71	-35 28 34.34	-	-	-	-	39.00 ^{+0.07} _{-0.06}	8.66/14	52.11 ± 0.49	33.46 ± 2.07	-0.19	-
11	3 38 20.05	-35 24 46.51	-	-	-	21.505±0.003	38.94 ^{+0.08} _{-0.08}	11.47/11	37.65 ± 0.67	12.41 ± 2.87	-0.48	-
12	3 38 33.42	-35 23 2.62	-	-	-	-	38.84 ^{+0.12} _{-0.11}	4.63/5	17.71 ± 0.53	15.60 ± 2.79	-0.06	-
13	3 38 31.90	-35 26 49.04	21.061±0.011	21.992±0.009	20.994±0.014	21.757±0.007	38.76 ^{+0.20} _{-0.10}	11.90/9	42.37 ± 0.83	25.00 ± 1.98	-0.23	1.048
14	3 38 33.82	-35 25 56.43	19.373±0.002	20.984±0.003	19.171±0.003	20.216±0.002	38.35 ^{+0.15} _{-0.14}	3.51/3	16.30 ± 0.51	< 8.76	< -0.27	1.813
15	3 38 38.80	-35 25 54.39	20.025±0.003	21.854±0.007	19.75±0.004	21.005±0.002	38.56 ^{+0.58} _{-0.14}	3.71/2	12.30 ± 0.41	5.94 ± 1.88	-0.32	2.104
16	3 38 36.83	-35 27 46.75	21.990±0.012	23.345±0.020	21.503±0.013	22.545±0.007	38.78 ^{+0.14} _{-0.09}	9.73/9	7.41 ± 0.42	< 5.38	< -0.14	1.842

Note. — (1) Source Number; (2) Right Ascension (J2000); (3) Declination (J2000); (4)-(7) Vega magnitudes in the HST F814W, F475W, F850LP and F606W filters; (8) unabsorbed X-ray luminosity (ergs/s); (9) χ^2 value for X-ray model used to estimate the luminosity; (10), (11) IR flux in MJy for the $3.6\mu\text{m}$ and $5.8\mu\text{m}$ bands; (12) mid-IR flux ratio; (13) optical ($g-z$) color. The ‘-’ sign denotes the cases where sources are not in the FOV of the HST image.

Table 3. Properties of X-ray sources without mid-IR counterparts.

No (1)	R.A. (2)	Dec. (3)	m _{814W} (4)	m _{475W} (5)	m _{850LP} (6)	m _{606W} (7)	L_X (8)	χ^2/dof (9)	3.6 μm (10)	5.8 μm (11)	$g - z$ (12)
17.	3 38 31.82	-35 26 3.76	21.132±0.008	22.901±0.015	20.882±0.010	21.786±0.023	39.10 ^{+0.04} _{-0.04}	25.14/27	<1.69	<6.32	2.019
18.	3 38 27.64	-35 26 48.16	<25.121	<26.253	<24.339	<26.468	39.29 ^{+0.09} _{-0.14}	44.34/30	<6.70	<8.84	-
19.	3 38 29.68	-35 25 4.10	-	-	-	-	39.01 ^{+0.11} _{-0.12}	8.22/9	<1.66	<8.80	-
20.	3 38 21.91	-35 29 28.30	-	-	-	-	38.95 ^{+0.11} _{-0.11}	14.96/9	<0.92	<5.57	-
21.	3 38 31.73	-35 30 58.65	-	-	-	-	38.42 ^{+0.17} _{-0.09}	5.96/5	<0.84	<4.97	-
22.	3 38 26.50	-35 27 31.91	<25.402	<26.883	<25.343	<27.266	38.71 ^{+0.11} _{-0.11}	9.00/7	<2.33	<6.48	-
23.	3 38 32.80	-35 26 58.29	21.703±0.017	23.184±0.022	21.457±0.022	22.546±0.011	38.74 ^{+0.16} _{-0.19}	5.39/7	<1.89	<5.53	1.727
24.	3 38 31.28	-35 24 12.12	-	-	-	-	38.95 ^{+0.48} _{-0.33}	2.35/2	<1.47	<8.42	-
25.	3 38 42.42	-35 24 0.60	-	-	-	-	38.73 ^{+0.12} _{-0.13}	3.31/3	<1.95	<11.64	-
26.	3 38 15.45	-35 26 29.05	-	-	-	-	38.52 ^{+0.50} _{-0.11}	6.21/4	<1.41	<8.33	-
27.	3 38 32.35	-35 27 1.75	23.213±0.07	24.562±0.078	23.061±0.091	23.885±0.041	38.47 ^{+0.76} _{-0.53}	2.98/5	<2.13	<5.45	1.501
28.	3 38 33.80	-35 26 57.96	21.058±0.008	22.946±0.016	20.762±0.010	22.067±0.006	39.03 ^{+2.95} _{-1.06}	0.46/2	<1.75	<5.62	2.184
29.	3 38 25.28	-35 27 52.97	20.519±0.004	22.37±0.009	20.255±0.006	21.52±0.004	38.62 ^{+0.15} _{-0.17}	2.08/3	<1.87	<6.41	2.115
30.	3 38 27.17	-35 26 0.91	20.434±0.004	22.319±0.010	20.137±0.006	21.479±0.004	38.71 ^{+0.25} _{-0.23}	5.29/3	<1.85	<9.17	2.182
31.	3 38 27.87	-35 25 26.85	<26.372	<26.803	<25.696	<27.361	38.31 ^{+0.48} _{-0.32}	2.53/4	<1.49	<6.79	-
32.	3 38 11.65	-35 26 48.41	-	-	-	-	38.68 ^{+0.10} _{-0.29}	0.85/4	<1.35	<7.34	-
33.	3 38 31.68	-35 26 0.22	20.814±0.006	22.789±0.014	20.464±0.008	21.836±0.005	38.49 ^{+0.09} _{-0.10}	6.76/10	<1.69	<6.30	2.325
34.	3 38 28.96	-35 26 2.0	23.456±0.064	24.836±0.091	23.023±0.066	24.343±0.042	38.77 ^{+0.19} _{-0.21}	5.49/8	<1.54	<5.42	1.813
35.	3 38 19.85	-35 28 45.48	-	-	-	-	38.40 ^{+0.57} _{-0.15}	4.82/3	<1.08	<5.87	-

Note. — (1) Source Number; (2) Right Ascension (J2000); (3) Declination (J2000); (4)-(7) Vega magnitudes in the HST F814W, F475W, F850LP, and F606W filters; (8) X-ray luminosity (ergs/s); (9) χ^2 value for X-ray model used to estimate the luminosity; (10), (11) IR flux in MJy for the 3.6 μm and 5.8 μm bands; (12) optical ($g - z$) color. The ‘-’ sign denote the cases where sources are not in the FOV of the HST image.

REFERENCES

- Agrawal V. K., Misra R., 2006, *ApJL*, 638, L83
- Allamandola L. J., Tielens A. G. G. M., Barker J. R., 1989, *ApJS*, 71, 733
- Angelini L., Loewenstein M., Mushotzky R. F., 2001, *ApJL*, 557, L35
- Asmus D., Gandhi P., Smette A., Hönig S. F., Duschl W. J., 2011, *A&A*, 536, A36
- Berghea C. T., Dudik R. P., Weaver K. A., Kallman T. R., 2010a, *ApJ*, 708, 354
- , 2010b, *ApJ*, 708, 364
- Bertin E., Arnouts S., 1996, *A&AS*, 117, 393
- Colbert E. J. M., Mushotzky R. F., 1999, *ApJ*, 519, 89
- Dale D. A. et al., 2006, *ApJ*, 646, 161
- Devi A. S., Misra R., Shanthi K., Singh K. Y., 2008, *ApJ*, 682, 218
- Dewangan G. C., Griffiths R. E., Rao A. R., 2006, *ApJL*, 641, L125
- Dewangan G. C., Misra R., Rao A. R., Griffiths R. E., 2010, *MNRAS*, 407, 291
- Dewangan G. C., Titarchuk L., Griffiths R. E., 2006, *ApJL*, 637, L21
- Feng H., Kaaret P., 2006, *ApJL*, 650, L75
- Feng H., Rao F., Kaaret P., 2010, *ApJL*, 710, L137
- Feng H., Soria R., 2011, *NewAR*, 55, 166
- Goad M. R., Roberts T. P., Knigge C., Lira P., 2002, *MNRAS*, 335, L67
- Hao L. et al., 2005, *ApJL*, 625, L75
- Harrison T. E., McNamara B. J., Bornak J., Gelino D. M., Wachter S., Rupen M. P., Gelino C. R., 2011, *ApJ*, 736, 54
- Hatziminaoglou E. et al., 2005, *AJ*, 129, 1198
- Houck J. R. et al., 2005, *ApJL*, 622, L105
- Jithesh V., Jeena K., Misra R., Ravindranath S., Dewangan G. C., Ravikumar C. D., Babu B. R. S., 2011, *ApJ*, 729, 67
- Kennicutt, Jr. R. C., 1998, *araa*, 36, 189
- Kennicutt, Jr. R. C. et al., 2003, *PASP*, 115, 928
- Kim D. et al., 2009, *ApJ*, 703, 829
- Kim E., Kim D., Fabbiano G., Lee M. G., Park H. S., Geisler D., Dirsch B., 2006, *ApJ*, 647, 276
- King A. R., 2008, *MNRAS*, 385, L113
- Krabbe A., Böker T., Maiolino R., 2001, *ApJ*, 557, 626
- Kubota A., Mizuno T., Makishima K., Fukazawa Y., Kotoku J., Ohnishi T., Tashiro M., 2001, *ApJL*, 547, L119
- Kuncic Z., Soria R., Hung C. K., Freeland M. C., Bicknell G. V., 2007, in *IAU Symposium*, Vol. 238, *IAU Symposium*, Karas V., Matt G., eds., pp. 247–250
- Kuntz K. D., Gruendl R. A., Chu Y., Chen C., Still M., Mukai K., Mushotzky R. F., 2005, *ApJL*, 620, L31
- Lacy M. et al., 2004, *ApJS*, 154, 166
- Leger A., Puget J. L., 1984, *A&A*, 137, L5
- Liu J., Bregman J., Miller J., Kaaret P., 2007, *ApJ*, 661, 165
- Liu J., Bregman J. N., Seitzer P., 2002, *ApJL*, 580, L31
- , 2004, *ApJ*, 602, 249
- Lutz D., Maiolino R., Spoon H. W. W., Moorwood A. F. M., 2004, *A&A*, 418, 465
- Makishima K. et al., 2000, *ApJ*, 535, 632
- Matsuta K. et al., 2012, *ApJ*, 753, 104
- Miller J. M., Fabbiano G., Miller M. C., Fabian A. C., 2003, *ApJL*, 585, L37
- Miller J. M., Fabian A. C., Miller M. C., 2004, *ApJ*, 607, 931
- Muno M. P., Mauerhan J., 2006, *ApJL*, 648, L135
- Paolillo M., Puzia T. H., Goudfrooij P., Zepf S. E., Maccarone T. J., Kundu A., Fabbiano G., Angelini L., 2011, *ApJ*, 736, 90
- Polletta M. d. C. et al., 2006, *ApJ*, 642, 673
- Ptak A., Colbert E., van der Marel R. P., Roye E., Heckman T., Towne B., 2006, *ApJS*, 166, 154
- Ramsey C. J., Williams R. M., Gruendl R. A., Chen C., Chu Y., Wang Q. D., 2006, *ApJ*, 641, 241
- Rao F., Feng H., Kaaret P., 2010, *ApJ*, 722, 620
- Russell D. M., Fender R. P., Hynes R. I., Brocksopp C., Homan J., Jonker P. G., Buxton M. M., 2006, *MNRAS*, 371, 1334
- Shakura N. I., Sunyaev R. A., 1973, *A&A*, 24, 337
- Stern D. et al., 2005, *ApJ*, 631, 163
- Stobbart A.-M., Roberts T. P., Wilms J., 2006, *MNRAS*, 368, 397
- Stoeckle J. T., Morris S. L., Gioia I. M., Maccacaro T., Schild R., Wolter A., Fleming T. A., Henry J. P., 1991, *ApJs*, 76, 813
- Strohmayer T. E., Mushotzky R. F., 2003, *ApJL*, 586, L61
- Strohmayer T. E., Mushotzky R. F., Winter L., Soria R., Uttley P., Cropper M., 2007, *ApJ*, 660, 580
- Swartz D. A., Ghosh K. K., Tennant A. F., Wu K., 2004, *ApJS*, 154, 519
- Symeonidis M. et al., 2011, *MNRAS*, 417, 2239
- Terashima Y., Inoue H., Wilson A. S., 2006, *ApJ*, 645, 264
- Tyler K., Quillen A. C., LaPage A., Rieke G. H., 2004, *ApJ*, 610, 213
- Vázquez G. A., Hornschemeier A. E., Colbert E., Roberts T. P., Ward M. J., Malhotra S., 2007, *ApJL*, 658, L21
- Wang Z. et al., 2004, *ApJS*, 154, 193
- Weedman D. W. et al., 2005, *ApJ*, 633, 706